DETECTION AND CLASSIFICATION OF STRUCTURAL CHANGES USING T-DISTRIBUTED STOCHASTIC NEIGHBOR EMBEDDING

Agis, D., Pozo, F.

Control, Modeling, Identification and Applications (CoDAlab), Department of Mathematics, Escola d'Enginyeria de Barcelona Est (EEBE), Universitat Politècnica de Catalunya (UPC), Campus Diagonal-Besòs (CDB), Eduard Maristany, 16, Barcelona 08019, Spain
francesc.pozo@upc.edu

ABSTRACT
This work states a structural health monitoring strategy for detection and classification of structural changes. The proposed approach is based on the so-called t-distributed stochastic neighbor embedding (t-SNE), a non-linear technique that is able to represent the local structure of high-dimensional data that are collected from multi-sensor signals in a simple scatter plot. All data sets were pre-processed using principal component analysis (PCA) to reduce their dimensionality before t-SNE was performed. More precisely, when a structure has to be diagnosed, the collected data from the current structure is projected into the t-SNE scatter plot. Subsequently, a sample of the projected data is compared with the center of the clusters of the pre-recorded damages. The current structure to be diagnosed is then associated with a damage based on the distances of the data to the centroids: the structure is classified based on the smallest point-centroid distance.
The methodology is evaluated using experimental data from an aluminum plate instrumented with piezoelectric transducers (PZTs). Results are presented in time domain, and they reveal the strong performance of t-SNE, with a percentage of correct decisions close to 100%.

KEYWORDS: Damage diagnosis, structural health monitoring, t-distributed stochastic neighbor embedding.

1. INTRODUCTION

Structural health monitoring (SHM) is an essential process for engineering structures because it verifies the correct functioning of the structure and determines whether it needs some kind of maintenance. Therefore, in SHM systems, detection and classification of structural changes are very important in order to know the current state of the structure for safety and to reduce maintenance costs. SHM has been applied in countless structures such as buildings [1], wind turbines [2, 3] and aircraft [4], among others, and a review of the state-of-the-art revealed that SHM is a very active research area.
In order to obtain information about the health state of the structure, data are collected from multi-sensor signals. The information extracted from multi-sensor signals creates a high-dimensional dataset that contains a large volume of data due to continuous measurements of the monitoring system. Several methods have been proposed for management high-dimensional, big and complex data. Among these methods, visualization techniques stand out as offer a way to handle this kind of data by means of an intuitive interface that allows people to easily detect natural clusters, identify hidden patterns, etc. [5]. And among visualization techniques, one of the most used is dimensionality reduction. Dimensionality reduction is the process of reducing the dimension of the original data, by keeping basically the same intrinsic information [6].
In the literature, various dimensionality reduction methods are proposed: (i) linear methods, that focus on keeping dissimilar original data points far apart in the low-dimensional space, such as principal component analysis (PCA) [7, 8, 9, 10, 11] and linear discriminant analysis (LDA) [10, 11]; and (ii) non-linear methods, that focus on keeping similar original data points close together in the low-dimensional space, such as isometric mapping (ISOMAP) [6, 9, 10], kernel PCA [8, 10] and t-distributed stochastic neighbor embedding (t-SNE) [12], among others.
This work proposes a SHM strategy for detection and classification of structural changes based on t-SNE, a technique developed by Laurens van der Maaten and Geoffrey Hinton [12], which is able to represent the local structure

of original high-dimensional data, obtained by the different sensors, in a low-dimensional space (for example a simple scatter plot). In a nutshell, in the low-dimensional space, each original high-dimensional point is represented by a low-dimensional point in such a way that nearby low-dimensional points correspond to similar original high-dimensional points, and distant low-dimensional points correspond to dissimilar original high-dimensional points. That is, this technique finds out patterns by identifying clusters based on similarity of data points. t-SNE has been applied to many real data (in the research area of stem cells [13], in computational linguistics [14], in astrophysics [15], in human genetics [16], etc.), but it should be noted that this is the first time that it has been applied in the field of SHM.

In this study, all data sets are pre-processed using PCA to reduce their dimensionality before t-SNE is performed. More precisely, when a structure has to be diagnosed, the collected data from the current structure is projected into the t-SNE scatter plot. Subsequently, a sample of the projected data is compared with the center of the clusters of the pre-recorded damages. The current structure to be diagnosed is then associated with a damage based on the distances of the data to the centroids: the structure is classified based on the smallest point-centroid distance.

The proposed methodology is evaluated using experimental data from an aluminum plate instrumented with piezoelectric transducers (PZTs) attached to its surface. Results are presented in time domain, and they show the high classification accuracy and the strong performance of t-SNE, with a percentage of correct decisions close to 100%. We must highlight that the environmental conditions were not considered, leaving it for future researches.

The contribution of this paper is that t-SNE is extended and adapted for the first time to the field of structural health monitoring, in detection and classification of structural changes, thanks to the developed methodology.

The structure of the paper is as follows: in Section 2, a brief description of the experimental setup is presented. Section 3 describes the damage classification strategy that is applied to classify the damage in the structure. In Section 4, the results are shown. Section 5, conclusions, closes the paper.

2. DESCRIPTION OF THE EXPERIMENTAL SETUP

2.1. Structure

In this work, an aluminum plate with an area of 40 cm^2 and with four piezoelectric transducers is consider to demonstrate the reliability of the damage detection and classification methodology introduced in Section 3. The location of the PZTs and of the three damages that are added in the structure are shown in Figure 1.

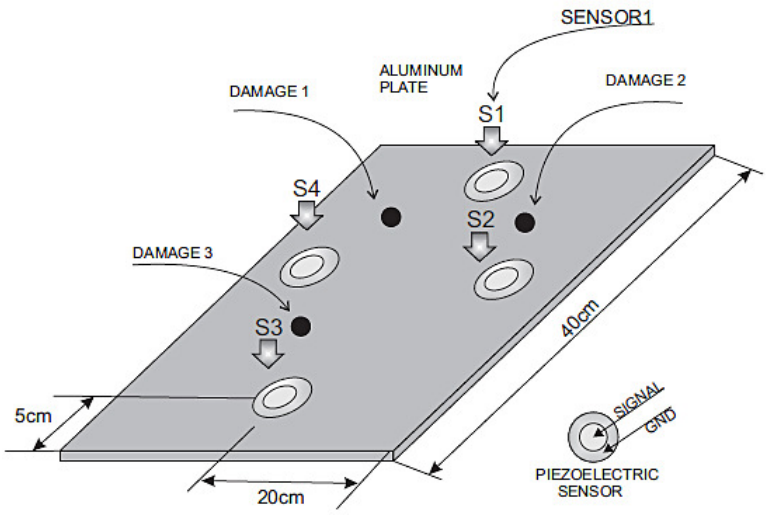

Figure 1 – Aluminum plate instrumented with four piezoelectric sensors. Source: Vitola et al. (2017a) [17].

2.2. Scenarios

The experimental setup includes three different scenarios to determine the behavior of the methodology:

- Scenario 1. The signals are acquired using a short cable (0.5 m) from the digitizer to the sensors, and these signals are filtered with a Golay filter algorithm after adding white Gaussian noise.
- Scenario 2. The signals are acquired using a long cable (2.5 m) to sensors, and signals are filtered with the Golay algorithm.

- Scenario 3. The signals are acquired using a short cable (0.5 m) from the digitizer to the sensors, and these signals are filtered without a Golay filter algorithm.

In this way, we can observe the effect of the attenuation with short and long cables, the effect of adding white Gaussian noise to the measured signals and the effect of the use of a Golay filter in the detection and classification process.

2.3. Sensors

A piezoelectric sensor network is used to excite the aluminum plate and collect the measured response. This sensor network works in several actuation phases. In each actuation phase, a PZT is used as actuator, and the rest of the PZTs are used as sensors. These data are organized in a matrix per actuator.

2.4. Damages

A mass is added to simulate the damage in the aluminum plate. This mass is an attached magnet in both sides of the plate to change its properties and produce changes in the propagated wave. The location of the mass defines each damage or structural state: Damage 1 ($D1$), Damage 2 ($D2$), Damage 3 ($D3$) and no damage ($D0$, healthy plate). Figure 2 shows these four structural states.

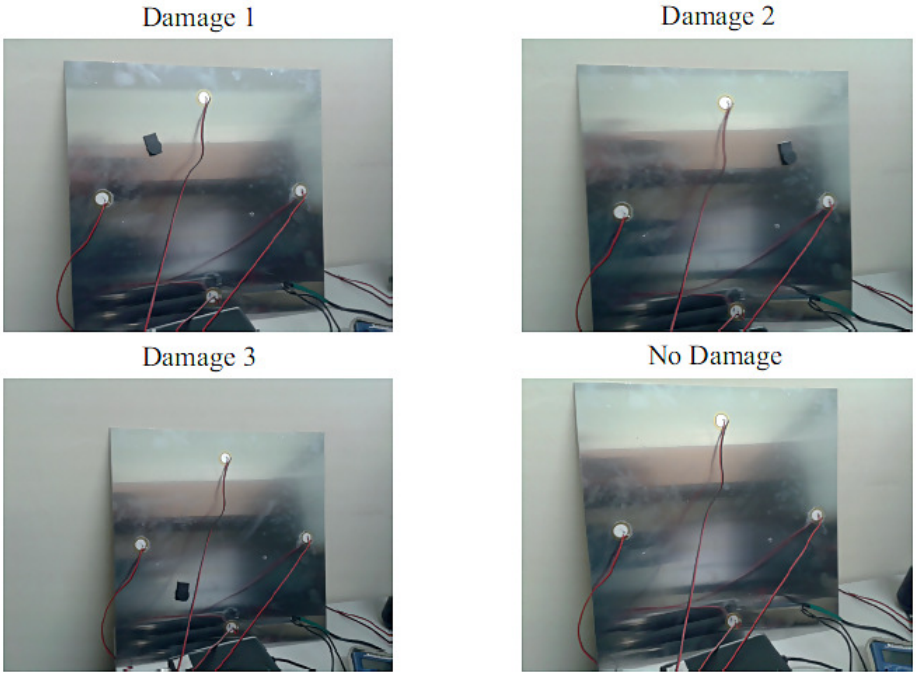

Figure 2 – Aluminum plate with four PZTs and with four different damages. Source: Vitola et al. (2017a) [17].

3. DAMAGE CLASSIFICATION STRATEGY

This work proposes a damage classification strategy that is based on the technique t-distributed stochastic neighbor embedding. This strategy will be described in the following subsections in more detail.

In a few words, all data sets —the data collected from the pristine structure and the new data coming from the structure to be diagnosed in an unknown state— are pre-processed using mean-centered group scaling (MCGS) and principal component analysis. Later, t-SNE is performed. Finally, confusion matrix is obtained from the distances of the data to the centroids associated with each structural state. More precisely, when a structure has to be diagnosed, the collected data from the current structure is projected into the t-SNE scatter plot. Subsequently, a sample of the projected data is compared with the center of the clusters of the pre-recorded damages. The current structure to be diagnosed is then associated with a damage based on the minimum distance to a cluster.

3.1. Data collection

The strategy uses data from an aluminum plate with four PZTs. Each PZT can operate as actuator —exciting the plate with a excitation signal— or as sensor —measuring signals. The number of PZTs defines the number of actuation phases, and each actuation phase defines a particular PZT as actuator and the rest of the PZTs as sensors:

Table 1 – Actuation phases.

Actuation phase	Actuator PZT	Sensor PZTs
1	1	2 – 3 – 4
2	2	1 – 3 – 4
3	3	1 – 2 – 4
4	4	1 – 2 – 3

Four data files are obtained from each scenario, one for each actuation phase. Each file is organized as follows: 25 experiments are performed for each structural state. Consequently, each file consists of 100 rows (25 experiments $\times$ 4 structural states). That is, the first 25 rows are captured without damage, the next 25 with Damage 1, the next 25 with Damage 2 and, finally, the last 25 with Damage 3. Regarding the columns, 60000 measurements are performed for each PZT that works as sensor. Therefore, each file contains 180000 columns (60000 measurements $\times$ 3 sensors). In matrix notation, the data are represented as follows:

$$\mathbf{Z}^{(i)} = \begin{pmatrix} z^{(i)}_{1,1} & z^{(i)}_{1,2} & \cdots & z^{(i)}_{1,180000} \\ z^{(i)}_{2,1} & z^{(i)}_{2,2} & \cdots & z^{(i)}_{2,180000} \\ \vdots & \vdots & \ddots & \vdots \\ z^{(i)}_{100,1} & z^{(i)}_{100,2} & \cdots & z^{(i)}_{100,180000} \end{pmatrix} \in \mathscr{M}_{100\times 180000}(\mathbb{R}), \tag{1}$$

where $i = 1,\ldots,4$ is the $i-$th actuation phase.
Finally, the data from all the actuation phases are stored in a matrix $\mathbf{Z}$:

$$\mathbf{Z} = \left(\mathbf{Z}^{(1)},\ldots,\mathbf{Z}^{(4)}\right) \in \mathscr{M}_{100\times(180000\cdot 4)}(\mathbb{R}) = \mathscr{M}_{100\times 720000}(\mathbb{R}), \tag{2}$$

this allows to analyze the information of all the actuation phases at one time. Figure 3 shows schematically the organization of the data captured in each scenario.

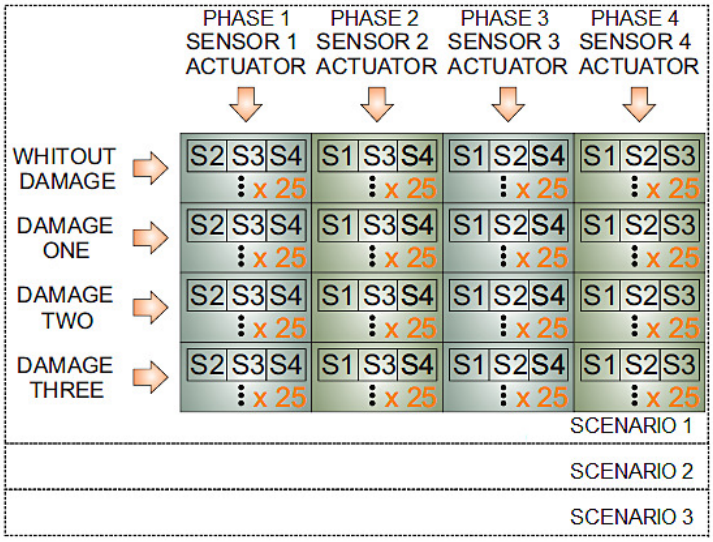

Figure 3 – Data organization per each scenario. Source: modified from Vitola et al. (2017b) [18].

3.2. Baseline data and test data

To obtain the baseline data and test data of this experimental study, a 5-fold cross validation is performed with matrix $\mathbf{Z}$, see Equation (2), to estimate the overall accuracy and avoid overfitting. In each iteration, the baseline

data, matrix $\mathbf{X}$, are obtained with 5 consecutive rows of each structural state of $\mathbf{Z}$, and with the rest of the rows of each state, 20, the test data, matrix $\mathbf{Y}$, is formed. For more details see Table 2.

Table 2 – Baseline data and test data obtained with 5-fold Cross Validation.

Iteration	Rows of each structural state of $\mathbf{Z}$ that form baseline data, $\mathbf{X}$	Rows of each structural state of $\mathbf{Z}$ that form test data, $\mathbf{Y}$
1	1:5	6:25
2	6:10	1:5 y 11:25
3	11:15	1:10 y 16:25
4	16:20	1:15 y 21:25
5	21:25	1:20

Therefore, from the matrix $\mathbf{Z}$, defined in Equation (2), five matrices $\mathbf{X} \in \mathscr{M}_{20\times 720000}(\mathbb{R})$ and five matrices $\mathbf{Y} \in \mathscr{M}_{80\times 720000}(\mathbb{R})$ are obtained, whose arrangement of their rows is:

Table 3 – Rows of matrices $\mathbf{X}$ and $\mathbf{Y}$.

Rows		Structural
$\mathbf{X}$	$\mathbf{Y}$	state
1:5	1:20	$D0$
6:10	21:40	$D1$
11:15	41:60	$D2$
16:20	61:80	$D3$

In matrix notation, the baseline data are represented as follows:

$$\mathbf{X} = \left(\begin{array}{ccc|ccc|c|ccc} x_{1,1}^{1,1} & \cdots & x_{1,1}^{1,60000} & x_{1,1}^{2,1} & \cdots & x_{1,1}^{2,60000} & \cdots & x_{1,1}^{12,1} & \cdots & x_{1,1}^{12,60000} \\ \vdots & \ddots & \vdots & \vdots & \ddots & \vdots & \ddots & \vdots & \ddots & \vdots \\ x_{5,1}^{1,1} & \cdots & x_{5,1}^{1,60000} & x_{5,1}^{2,1} & \cdots & x_{5,1}^{2,60000} & \cdots & x_{5,1}^{12,1} & \cdots & x_{5,1}^{12,60000} \\ \vdots & \ddots & \vdots & \vdots & \ddots & \vdots & \ddots & \vdots & \ddots & \vdots \\ x_{1,4}^{1,1} & \cdots & x_{1,4}^{1,60000} & x_{1,4}^{2,1} & \cdots & x_{1,4}^{2,60000} & \cdots & x_{1,4}^{12,1} & \cdots & x_{1,4}^{12,60000} \\ \vdots & \ddots & \vdots & \vdots & \ddots & \vdots & \ddots & \vdots & \ddots & \vdots \\ x_{5,4}^{1,1} & \cdots & x_{5,4}^{1,60000} & x_{5,4}^{2,1} & \cdots & x_{5,4}^{2,60000} & \cdots & x_{5,4}^{12,1} & \cdots & x_{5,4}^{12,60000} \end{array}\right), \tag{3}$$

where each element of that matrix

$$x_{i,l}^{k,j}, \quad k = 1,\ldots,12, \quad j = 1,\ldots,60000, \quad i = 1,\ldots,5, \quad l = 1,\ldots,4, \tag{4}$$

comes from the $j-$th measurement of the $k-$th sensor of the $l-$th structural state in the $i-$th experiment. Summarizing, there are 12 sensors, 60000 measurements per sensor, 4 structural states and 5 rows associated with each structural state.
In matrix notation, the test data are represented as follows:

$$\mathbf{Y} = \left(\begin{array}{ccc|ccc|c|ccc} y_{1,1}^{1,1} & \cdots & y_{1,1}^{1,60000} & y_{1,1}^{2,1} & \cdots & y_{1,1}^{2,60000} & \cdots & y_{1,1}^{12,1} & \cdots & y_{1,1}^{12,60000} \\ \vdots & \ddots & \vdots & \vdots & \ddots & \vdots & \ddots & \vdots & \ddots & \vdots \\ y_{20,1}^{1,1} & \cdots & y_{20,1}^{1,60000} & y_{20,1}^{2,1} & \cdots & y_{20,1}^{2,60000} & \cdots & y_{20,1}^{12,1} & \cdots & y_{20,1}^{12,60000} \\ \vdots & \ddots & \vdots & \vdots & \ddots & \vdots & \ddots & \vdots & \ddots & \vdots \\ y_{1,4}^{1,1} & \cdots & y_{1,4}^{1,60000} & y_{1,4}^{2,1} & \cdots & y_{1,4}^{2,60000} & \cdots & y_{1,4}^{12,1} & \cdots & y_{1,4}^{12,60000} \\ \vdots & \ddots & \vdots & \vdots & \ddots & \vdots & \ddots & \vdots & \ddots & \vdots \\ y_{20,4}^{1,1} & \cdots & y_{20,4}^{1,60000} & y_{20,4}^{2,1} & \cdots & y_{20,4}^{2,60000} & \cdots & y_{20,4}^{12,1} & \cdots & y_{20,4}^{12,60000} \end{array}\right), \tag{5}$$

where each element of that matrix

$$y_{i,l}^{k,j}, \quad k=1,\ldots,12, \quad j=1,\ldots,60000, \quad i=1,\ldots,20, \quad l=1,\ldots,4, \tag{6}$$

comes from the $j-$th measurement of the $k-$th sensor of the $l-$th "unknown" structural state to be diagnosed in the $i-$th experiment.

3.3. Mean-centered group scaling (MCGS)

The data in matrix $\mathbf{X}$ are normalized by mean-centered group scaling method [19]. The main reasons to normalize the raw data are two: (i) data come from several sensors and could have different scales; and (ii) to simplify the computations in the PCA decomposition. MCGS is based on the mean of all experiments of the sensor at the same column and the standard deviation of all experiments of the sensor. More accurately, it is defined:

$$\mu^{k,j} = \frac{1}{n}\sum_{l=1}^{4}\sum_{i=1}^{5} x_{i,l}^{k,j}, \quad n=5 \text{ rows} \times 4 \text{ structural states} = 20, \quad k=1,\ldots,12, \quad j=1,\ldots,60000, \tag{7}$$

$$\sigma^{k} = \sqrt{\frac{1}{n\cdot 60000}\sum_{l=1}^{4}\sum_{i=1}^{5}\sum_{j=1}^{60000}(x_{i,l}^{k,j}-\mu^{k})^2}, \quad k=1,\ldots,12, \tag{8}$$

$$\mu^{k} = \frac{1}{n\cdot 60000}\sum_{l=1}^{4}\sum_{i=1}^{5}\sum_{j=1}^{60000} x_{i,l}^{k,j}, \quad k=1,\ldots,12, \tag{9}$$

where $\mu^{k,j}$ is the arithmetic mean of data that are at the same column, that is the arithmetic mean of the n experiments of $k-$th sensor in $j-$th measure; and σ^k and μ^k are the standard deviation and the arithmetic mean of all experiments of sensor k, respectively. Then, the elements $x_{i,l}^{k,j}$ of matrix $\mathbf{X}$ are normalized to define a new matrix $\breve{\mathbf{X}} = \mathbf{X}_{MCGS} = (\breve{x}_{i,l}^{k,j})$ as:

$$\breve{x}_{i,l}^{k,j} := \frac{x_{i,l}^{k,j}-\mu^{k,j}}{\sigma^{k}}, \;\; k=1,\ldots,12, \;\; j=1,\ldots,60000, \;\; i=1,\ldots,5, \;\; l=1,\ldots,4, \tag{10}$$

One of the properties of the normalized matrix $\breve{\mathbf{X}}$ is that each column has an arithmetic mean of zero and that all experiments of sensor k have a standard deviation of one.

Then, the test data are processed in an identical manner as the baseline data. This means that these data are normalized by MCGS, but respect to data $\mathbf{X}$:

$$\breve{y}_{i,l}^{k,j} := \frac{y_{i,l}^{k,j}-\mu^{k,j}}{\sigma^{k}}, \;\; k=1,\ldots,12, \;\; j=1,\ldots,60000, \;\; i=1,\ldots,20, \;\; l=1,\ldots,4, \tag{11}$$

obtaining the matrix $\breve{\mathbf{Y}}$, and where $\mu^{k,j}$ and σ^k are defined in Equations (7) and (8), respectively.

3.4. Principal component analysis (PCA)

In the next step, the normalized baseline data, $\breve{\mathbf{X}}$, are pre-processed using PCA [20] to reduce its dimensionality before performing t-SNE. The main objective of PCA is to reduce the calculation time in t-SNE. By using PCA with $\breve{\mathbf{X}}$, PCA model is obtained, that is, the square matrix $\mathbf{P} \in \mathscr{M}_{720000\times 720000}(\mathbb{R})$ used to project the data stored in $\breve{\mathbf{X}}$ and $\breve{\mathbf{Y}}$ with the corresponding matrix product:

$$\mathbf{T}_1 = \breve{\mathbf{X}}\cdot\mathbf{P} \in \mathscr{M}_{20\times 720000}(\mathbb{R}), \tag{12}$$

$$\mathbf{T}_2 = \breve{\mathbf{Y}}\cdot\mathbf{P} \in \mathscr{M}_{80\times 720000}(\mathbb{R}). \tag{13}$$

3.5. Projected data fusion

The projected data are assembled, that is:

$$\mathbf{T} = \begin{pmatrix} \mathbf{T}_1 \\ \mathbf{T}_2 \end{pmatrix} \in \mathscr{M}_{(20+80)\times 720000}(\mathbb{R}), \tag{14}$$

so $\mathbf{T}$ has 100 points in a space of dimension $\mathbb{R}^{720000}$. In this case, a single row of $\mathbf{T}_2$ is added each time, i.e., $\mathbf{T}$ has $20+1=21$ points. This new row introduced represents the new datum from the structure to be diagnosed, which is in an "unknown" state. This means that we try to classify the structural state of a system one at a time.

3.6. t-Distributed stochastic neighbor embedding (t-SNE)

t-SNE is an improved variation of the technique so-called stochastic neighbor embedding (SNE) [9]: t-SNE is much easier to optimize and produces better visualizations, since it reduces the tendency to crowd points in the center of the distribution (the so-called *crowding problem*[1]). These improvements are due to the fact that the cost function used by t-SNE differs from the one used by SNE in two aspects: (i) t-SNE uses a symmetrized version of the SNE cost function with simpler gradients; and (ii) t-SNE uses a t-Student distribution, instead of a Gaussian, to compute the similarity between two points in the low-dimensional space.

Following with the proposed strategy, t-SNE is executed with the matrix $\mathbf{T}$, obtaining a succession of 21 points in the plane $\mathbb{R}^2$. The result of t-SNE in the final iteration is such that:

$$\mathbf{S} = \left(\begin{array}{ccc|c|ccc|c} s^1_{1,1} & \cdots & s^1_{5,1} & \cdots & s^4_{1,1} & \cdots & s^4_{5,1} & s_{1,1} \\ s^1_{1,2} & \cdots & s^1_{5,2} & \cdots & s^4_{1,2} & \cdots & s^4_{5,2} & s_{1,2} \end{array} \right)^{\mathsf{T}}, \tag{15}$$

where the element $s^l_{i,j}$ corresponds to the $j-$th measurement of $l-$th structural state of the $i-$th experiment. The last element of each row correspond to the "unknown" structural state to be diagnosed. A brief description of key mathematical and statistical concepts of t-SNE is introduced below.

3.6.1. *t-SNE: brief description*

Given a collection of high-dimensional data points $X = \{x_1, ..., x_n\} \subset \mathbb{R}^D$, the objective is to find a collection of low-dimensional map points $Y = \{y_1, ..., y_n\} \subset \mathbb{R}^d$ (typical values for d are 2 or 3), where $d \ll D$, such that the lower dimension preserves, as much as possible, the local structure of the original data X. That is, if two data points are neighbors, it wants the two corresponding map points also to be neighbors. To this end, t-SNE first converts the high-dimensional Euclidean distances between data points x_i and x_j, $\|x_i - x_j\|$, into conditional probabilities by centering a Gaussian distribution at x_i, computing the density of x_j under this Gaussian distribution, and renormalizing:

$$p_{j|i} = \frac{\exp(-\|x_i - x_j\|^2/2\sigma_i^2)}{\sum_{k \neq i} \exp(-\|x_i - x_k\|^2/2\sigma_i^2)}, \quad \forall i \forall j : i \neq j, \tag{16}$$

where $\|x_i - x_j\|^2/2\sigma_i^2$ (scaled squared Euclidean distance or "affinity") is the dissimilarity between data points x_i and x_j. The variance of the Gaussian distribution, σ_i^2, is calculated automatically (for more details, see the original t-SNE paper [12]). Since only pairwise similarities between data points are of interest, t-SNE establishes $p_{i|i} = 0$. This conditional probability measures the similarity of x_j to x_i, i.e., the probability that x_i would pick x_j as its neighbor. If two data points are near, $p_{j|i}$ will be high. Whereas if two data points are separated, $p_{j|i}$ will be low.

Then, by symmetrizing two conditional probabilities, t-SNE defines the joint probability, that is a symmetrized version of the conditional similarity because it has the property that $p_{ij} = p_{ji}$ for $\forall i, j$:

$$p_{ij} = \frac{p_{j|i} + p_{i|j}}{2n}, \quad p_{ii} = 0. \tag{17}$$

The joint probability also measures the pairwise similarity between data points x_i and x_j. Thus it is obtained the similarity matrix $\mathbf{P}$ for high-dimensional data points. In practice, the use of conditional or joint probabilities produces similar results, but it is less computationally expensive the optimization of the joint model [12]. The objective of t-SNE is to model each data point x_i by a map point y_i such that the pairwise similarities p_{ij} are modeled as well as possible in the low-dimensional space.

Once obtained the similarity matrix for the data points X, let's also define the similarity matrix $\mathbf{Q}$ for the map points Y. It is the same idea as for the data points, but with a renormalized t-Student distribution with one degree of freedom and $\sigma_i^2 = \frac{1}{2}$ for all i, instead of a Gaussian distribution:

$$q_{ij} = \frac{(1 + \|y_i - y_j\|^2)^{-1}}{\sum_k \sum_{l \neq k} (1 + \|y_k - y_l\|^2)^{-1}}, \quad \forall i \forall j : i \neq j, \quad q_{ii} = 0, \quad q_{ij} = q_{ji} \forall i, j, \tag{18}$$

i.e., q_{ij} is the low-dimensional counterpart of p_{ij} and it represents the local structure of the data points in the low-dimensional space. The heavy tails of the t-Student distribution allow dissimilar data points x_i and x_j to be modeled by map points y_i and y_j that are separated: the probability of being neighbor falls off more slowly and therefore there is less need to move some points away and crowd remaining points in the center of the distribution (*crowding problem*). In other words, t-SNE allows data points that are only slightly similar to be visualized more

[1] SNE suffers from a *crowding problem* that is the result of the exponential volume difference between high and low-dimensional spaces [12].

separated in the low-dimensional space. But the choice of the t-Student distribution for the map points goes further since it alleviates both the crowding problem and the optimization problems of SNE [12].
Whereas the similarity matrix **P** is fixed, the similarity matrix **Q** depends on the map points, and what is wanted is that these two similarity matrices are closer as possible. This is achieved by minimizing a cost function which is the Kullback-Leibler (KL) divergence between both joint distributions [9, 10, 12]:

$$C = KL(P\|Q) = \sum_i \sum_{j \neq i} p_{ij} \log \frac{p_{ij}}{q_{ij}}. \tag{19}$$

The KL divergence between the joint probability distributions **P** and **Q** measures the distance between the two similarity matrices, and therefore minimizing the KL divergence reduces the error between these matrices. In other words, the map points of similar data points need to be close together and the map points of dissimilar data points need to be far in order to minimize the cost function C. Note that (i) KL divergence is nonnegative and 0 iff the distributions are equal —the similarity between the data points x_i and x_j is correctly modeled by the map points y_i and y_j—, and (ii) C is generally non-convex and different runs might produce different results. To minimize C, it is perform a gradient descent[2] method:

$$\frac{\partial C}{\partial y_i} = 4 \sum_{j \neq i} (p_{ij} - q_{ij})(y_i - y_j)(1 + \|y_i - y_j\|^2)^{-1}. \tag{20}$$

This gradient expresses the sum of all forces applied to map point y_i, i.e., the sum of forces pulling map point y_i toward all other map points y_j or pushing it away. And the locations of the map points Y are determined by minimizing C.
Then y_i is updated by the next equation:

$$y_i^{(t)} = y_i^{(t-1)} + \eta \frac{\partial C}{\partial y_i} + \alpha(t)(y_i^{(t-1)} - y_i^{(t-2)}), \tag{21}$$

where $y_i^{(t)}$ is the solution at iteration t, η is the learning rate, and $\alpha(t)$ is the momentum term at iteration t. The learning rate determines the jump size between each iteration during the optimization of the cost function C. In Equation (21), a relatively large momentum term is added to accelerate the optimization and to avoid poor local minimums.
t-SNE Summary:

1. Calculate the similarity matrix for the data points, p_{ij}.
2. Calculate the similarity matrix for the map points, q_{ij}.
3. Define the cost function, $C = KL(P\|Q)$.
4. Minimize C using gradient descent algorithm.
5. Update y_i using Equation (21).

3.7. Confusion matrix

The confusion matrices are calculated as of the distances of the points $(s_{1,1}, s_{1,2}) \subset \mathbb{R}^2$, to the centroids associated with each structural state. The centroid associated with the $l-$th structural state, $l = 1, \ldots, 4$, is the point of the plane such that

$$(c_x^l, c_y^l) = \left(\frac{1}{5} \sum_{i=1}^{5} s_{i,1}^l, \frac{1}{5} \sum_{i=1}^{5} s_{i,2}^l \right). \tag{22}$$

To classify this point of the plane, the smallest point-centroid distance is used: the distance of this point $(s_{1,1}, s_{1,2}) \subset \mathbb{R}^2$ is calculated up to each of the centroids defined in Equation (22) and it is classified as structural state $m \in \mathbb{N}$ if m is such that

$$\sqrt{(s_{1,1} - c_x^m)^2 + (s_{1,2} - c_y^m)^2} = \min_{l=1,\ldots,4} \sqrt{(s_{1,1} - c_x^l)^2 + (s_{1,2} - c_y^l)^2}. \tag{23}$$

4. RESULTS

Tables 4–6 present the classification results per scenario, in the time domain. Remember that of each damage or structural state there are 100 cases (20 rows of matrix $\mathbf{Y} \times 5$ iterations of 5-fold Cross Validation, see Tables 2

[2] Gradient descent: iterative process to find the minimal of a function

and 3). The results with maximum accuracy in the classification are obtained in scenarios 1 and 3: all cases have been correctly classified. In scenario 2, the percentage of correct decisions fluctuates between 86% and 91%: it can be observed that the use of a long cable (2.5 m) from the digitizer to the sensors affects in the detection and classification method. So that, the results show the high classification accuracy and the solid performance of t-SNE algorithm. It should be noted that the environmental conditions were not considered, leaving them for future researches.

Table 4 – Confusion matrix, scenario 1, time domain.

True \ Predicted	D0	D1	D2	D3
D0	100	0	0	0
D1	0	100	0	0
D2	0	0	100	0
D3	0	0	0	100

Table 5 – Confusion matrix, scenario 2, time domain.

True \ Predicted	D0	D1	D2	D3
D0	86	1	7	6
D1	8	88	4	0
D2	1	8	89	2
D3	3	4	2	91

Table 6 – Confusion matrix, scenario 3, time domain.

True \ Predicted	D0	D1	D2	D3
D0	100	0	0	0
D1	0	100	0	0
D2	0	0	100	0
D3	0	0	0	100

5. CONCLUSIONS

In this work, a methodology to detect and classify structural changes has been proposed. Results from an aluminum plate have shown that this method is very satisfactory, given its high classification accuracy, since the number of correct decisions fluctuates between 86% and 100%. In addition, it is worth remarking that the t-SNE technique has been extended and adapted for the first time to the field of structural health monitoring, in the detection and classification of structural changes, thanks to the developed methodology.

ACKNOWLEDGEMENTS

This work has been partially funded by the Spanish Agencia Estatal de Investigación (AEI) - Ministerio de Economía, Industria y Competitividad (MINECO), and the Fondo Europeo de Desarrollo Regional (FEDER) through the research project DPI2017-82930-C2-1-R; and by the Generalitat de Catalunya through the research project 2017 SGR 388. We gratefully acknowledge the support of NVIDIA Corporation with the donation of the Titan Xp GPU used for this research. We thank the Universitat Politècnica de Catalunya (UPC) for pre-doctoral fellowship (to Agis, D.).

REFERENCES

[1] Raju, K.S., Pratap, Y., Sahni, Y., Babu, M.N., "Implementation of a WSN system towards SHM of civil building structures", Proceedings of Intelligent Systems and Control (ISCO), 2015 IEEE 9th International Conference on, IEEE, 2015, pp. 1–7.

[2] Rolfes, R., Zerbst, S., Haake, G., Reetz, J., Lynch, J.P., "Integral SHM-system for offshore wind turbines using smart wireless sensors", Proceedings of Proceedings of the 6th International Workshop on Structural Health Monitoring, DEStech Publications Inc. Stanford, CA, USA, 2007, pp. 11–13.

[3] Ciang, C.C., Lee, J.R., Bang, H.J., "Structural health monitoring for a wind turbine system: a review of damage detection methods", Measurement Science and Technology, 19(12), 2008, p. 122001.

[4] Nisha, M., "Structural health monitoring of aircraft wing using wireless network", Int. J. Technol. Explor. Learn. www. ijtel. org Struct, 3(1), 2014, pp. 341–343.

[5] Ward, M.O., Grinstein, G., Keim, D., Interactive data visualization: foundations, techniques, and applications, AK Peters/CRC Press, 2015.

[6] Tenenbaum, J.B., De Silva, V., Langford, J.C., "A global geometric framework for nonlinear dimensionality reduction", Science, 290(5500), 2000, pp. 2319–2323.

[7] Kambhatla, N., Leen, T.K., "Dimension reduction by local principal component analysis", Neural Computation, 9(7), 1997, pp. 1493–1516.

[8] Cao, L., Chua, K.S., Chong, W., Lee, H., Gu, Q., "A comparison of PCA, KPCA and ICA for dimensionality reduction in support vector machine", Neurocomputing, 55(1-2), 2003, pp. 321–336.

[9] Hinton, G.E., Roweis, S.T., "Stochastic neighbor embedding", Proceedings of Advances in Neural Information Processing Systems, 2003, pp. 857–864.

[10] Min, R., A non-linear dimensionality reduction method for improving nearest neighbour classification, University of Toronto, 2005.

[11] Sharma, A., Paliwal, K.K., Onwubolu, G.C., "Class-dependent PCA, MDC and LDA: A combined classifier for pattern classification", Pattern Recognition, 39(7), 2006, pp. 1215–1229.

[12] Maaten, L.v.d., Hinton, G., "Visualizing data using t-SNE", Journal of Machine Learning Research, 9(Nov), 2008, pp. 2579–2605.

[13] Wilson, N.K., Kent, D.G., Buettner, F., Shehata, M., Macaulay, I.C., Calero-Nieto, F.J., Castillo, M.S., Oedekoven, C.A., Diamanti, E., Schulte, R., et al., "Combined single-cell functional and gene expression analysis resolves heterogeneity within stem cell populations", Cell Stem Cell, 16(6), 2015, pp. 712–724.

[14] Gouws, S., Søgaard, A., "Simple task-specific bilingual word embeddings", Proceedings of Proceedings of the 2015 Conference of the North American Chapter of the Association for Computational Linguistics: Human Language Technologies, 2015, pp. 1386–1390.

[15] Traven, G., Matijevič, G., Zwitter, T., Žerjal, M., Kos, J., Asplund, M., Bland-Hawthorn, J., Casey, A.R., De Silva, G., Freeman, K., et al., "The Galah survey: classification and diagnostics with t-SNE reduction of spectral information", The Astrophysical Journal Supplement Series, 228(2), 2017, p. 24.

[16] Li, W., Cerise, J.E., Yang, Y., Han, H., "Application of t-SNE to human genetic data", Journal of Bioinformatics and Computational Biology, 15(04), 2017, p. 1750017.

[17] Vitola, J., Pozo, F., Tibaduiza, D.A., Anaya, M., "A sensor data fusion system based on *k*-nearest neighbor pattern classification for structural health monitoring applications", Sensors, 17(2), 2017, p. 417.

[18] Vitola, J., Pozo, F., Tibaduiza, D.A., Anaya, M., "Distributed piezoelectric sensor system for damage identification in structures subjected to temperature changes", Sensors, 17(6), 2017, p. 1252.

[19] Pozo, F., Vidal, Y., Salgado, Ó., "Wind Turbine Condition Monitoring Strategy through Multiway PCA and Multivariate Inference", Energies, 11(4), 2018, p. 749.

[20] Pozo, F., Vidal, Y., "Wind turbine fault detection through principal component analysis and statistical hypothesis testing", Energies, 9(1), 2015, p. 3.